# Spectral holographic trapping: Creating dynamic force landscapes with polyphonic waves

Mia C. Morrell<sup>®</sup>, Julianne E. Lee<sup>®</sup>, and David G. Grier<sup>®</sup>1

<sup>1</sup>Department of Physics and Center for Soft Matter Research, New York University, New York, New York 10003, USA

<sup>2</sup>Cornell University, Ithaca, New York 14853, USA

(Received 20 November 2023; accepted 27 February 2024; published 2 April 2024)

Acoustic trapping uses forces exerted by sound waves to transport small objects along specified trajectories in three dimensions. The structure of the time-averaged acoustic force landscape acting on an object is determined by the amplitude and phase profiles of the sound's pressure wave. These profiles typically are sculpted by deliberately selecting the amplitude and relative phase of the sound projected by each transducer in large arrays of transducers, all operating at the same carrier frequency. This approach leverages a powerful analogy with holographic optical trapping at the cost of considerable technical complexity. Acoustic force fields also can be shaped by the spectral content of the component sound waves in a manner that is not feasible with light. The same theoretical framework that predicts the time-averaged structure of monotone acoustic force landscapes can be applied to spectrally rich sound fields in the quasistatic approximation, creating opportunities for dexterous control using comparatively simple hardware. We demonstrate this approach to spectral holographic acoustic trapping by projecting acoustic conveyor beams that move millimeter-scale objects along prescribed paths. Spectral control of reflections provides yet another opportunity for controlling the structure and dynamics of an acoustic force landscape. We use this approach to realize two variations on the theme of a wave-driven oscillator, a deceptively simple dynamical system with surprisingly complex phenomenology.

### DOI: 10.1103/PhysRevE.109.044901

# I. INTRODUCTION

Forces exerted by sound waves can levitate and transport small objects without physical contact, which is a boon for processing sensitive [1] and hazardous materials [2]. The interplay of sound waves with small scatterers also provides an archetypal model for investigating the physics of wave-matter composite systems [3–6]. Most implementations of acoustic trapping use sound waves of a single fixed frequency and achieve dexterous control by suitably structuring the waves' amplitude and phase profiles with large arrays of acoustic "pixels" [7,8]. Like holographic optical traps [9], this kind of acoustic trapping pattern is reconfigured by actively changing the amplitude and phase of the wave projected by each pixel in the array.

Here, we draw attention to an alternative approach to dynamic acoustic trapping whose ability to move matter along prescribed paths is encoded in the spectral content of a small number of acoustic sources. We illustrate the potential utility of such spectral holograms by demonstrating dynamic acoustic manipulation along a single axis using just two acoustic pixels emitting stationary sound fields.

Section I reviews relevant elements of the theory of acoustic forces and motivates the quasistatic approximation used to design spectral holograms. These principles are used in Sec. II to realize illustrative examples of dynamic acoustic force landscapes, including a unidirectional acoustic conveyor and a bidirectional acoustic scanner that are realized experimentally using the acoustic levitator depicted in Fig. 1. Experimental realizations of spectral holographic trapping also demonstrate a role for cavity resonances in creating structured force landscapes. Inertia and drag also contribute to the dynamics of

objects moving through acoustic force landscapes in low-viscosity media, such as air. Section III introduces methods to incorporate their influence and uses this formalism to describe the behavior of a wave-driven oscillator [10].

#### II. ACOUSTIC FORCES

A steady sound wave at frequency  $\omega$  propagating through a fluid medium can be characterized by the real-valued amplitude profile  $u(\mathbf{r})$  and phase profile  $\phi(\mathbf{r})$  of its pressure field:

$$p(\mathbf{r},t) = u(\mathbf{r}) e^{i\phi(\mathbf{r})} e^{-i\omega t}. \tag{1}$$

This structured wave can be decomposed into plane waves whose wave number satisfies the standard dispersion relation  $k = \omega/c_m$ , where  $c_m$  is the speed of sound in the medium. For simplicity, we assume that the pressure wave's amplitude is small enough that we may neglect the fluid's viscosity and treat the sound's propagation to be nondispersive and linear. This also means that we may neglect acoustic streaming in the medium, which is reasonable for acoustic levitation in air. Under these assumptions, the pressure acts as the scalar potential for the sound wave's velocity field:

$$\mathbf{v}(\mathbf{r},t) = -\frac{i}{\omega \rho_m} \nabla p, \tag{2}$$

where  $\rho_m$  is the density of the medium.

A small sphere of radius  $a_p$  at position r in this field experiences a time-averaged acoustic force [11,12],

$$\boldsymbol{F}(\boldsymbol{r}) = \frac{1}{2} \operatorname{Re} \left\{ \alpha \, p \boldsymbol{\nabla} p^* + \beta \, \sum_{j=1}^3 v_j \boldsymbol{\nabla} v_j^* \right\}, \quad (3a)$$

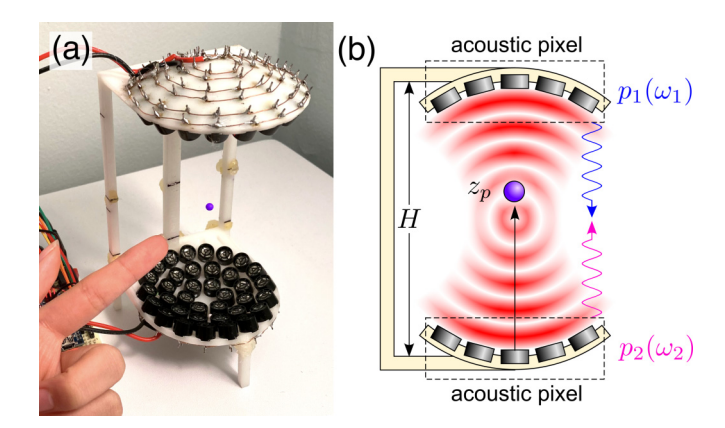


FIG. 1. (a) Acoustic trap holding a single millimeter-scale particle in air at a carrier frequency of  $f = \omega/(2\pi) = 40 \, \text{kHz}$ . (b) Schematic representation of spectral holographic trapping. Two acoustic pixels launch counterpropagating pressure waves,  $p_1(\omega_1)$  and  $p_2(\omega_2)$ , into a spherical cavity of height H defined by the boundaries of the transducer banks. Dense rigid particles can be trapped at nodes in the combined pressure field. The traps' positions evolve in time based on the spectral content of the two projected waves.

where  $\alpha$  and  $\beta$  are the particle's monopole and dipole polarizabilities, respectively. For a spherical particle of radius  $a_p$  composed of a material with density  $\rho_p$  and isentropic compressibility  $\kappa_p$  [11,12], the polarizabilities are

$$\alpha = \frac{4\pi}{3} a_p^3 \kappa_m f_0 \left[ -1 + \frac{i}{3} (f_0 + f_1)(ka_p)^3 \right], \quad (3b)$$

$$\beta = 2\pi a_p^3 \, \rho_m \, f_1 \left[ 1 + \frac{i}{6} f_1 (k a_p)^3 \right], \tag{3c}$$

where  $\kappa_m = (\rho_m c_m^2)^{-1}$  is the isentropic compressibility of the fluid medium, and where the monopole and dipole scattering coefficients are

$$f_0 = 1 - \frac{\kappa_p}{\kappa_m} \tag{3d}$$

and

$$f_1 = \frac{\rho_p - \rho_m}{\rho_p + \frac{1}{2}\rho_m},$$
 (3e)

respectively.

Substituting Eqs. (1) and (2) into Eq. (3) yields the time-averaged force on a sphere,

$$F(\mathbf{r}) = -\nabla U_G(\mathbf{r}) + \mathcal{O}\{(ka_p)^6\},\tag{4a}$$

where

$$U_G(\mathbf{r}) = A u^2 + B \frac{1}{k^2} \nabla^2 u^2$$
 (4b)

is the classic Gor'kov potential [12,13]. The coefficients,

$$A = \frac{\pi}{3} a_p^3 \kappa_m \left( f_0 - \frac{3}{2} f_1 \right)$$
 (4c)

and

$$B = -\frac{\pi}{4} a_p^3 \kappa_m f_1, \tag{4d}$$

are both negative for particles that are denser and less compressible than the medium. Such particles therefore are attracted to nodes of the pressure field.

The force landscape described by Eq. (4) depends on the pressure wave's amplitude rather than its phase and is manifestly conservative if  $u(\mathbf{r})$  is independent of time. The phase profile  $\phi(\mathbf{r})$  directs nonconservative acoustic radiation forces [12] whose prefactors scale with particle size as  $(ka_p)^6$  and therefore tend to be negligibly weak for subwavelength particles. Phase-gradient contributions to  $F(\mathbf{r})$  vanish identically in standing waves, which have no phase gradients.

Equation (3a) represents an average over one acoustic period [14]. The same expression approximately describes changes in the acoustic force landscape F(r) due to variations in the pressure wave's amplitude u(r,t), provided that those variations are sufficiently slow. This quasistatic approximation is valid when

$$\left| \frac{1}{u(\mathbf{r},t)} \frac{\partial u(\mathbf{r},t)}{\partial t} \right| \ll \omega, \tag{5}$$

which is satisfied when the bandwidth  $\Delta\omega$  of the waveform emitted by each acoustic pixel is much smaller than the center frequency  $\omega$ .

# III. DYNAMIC ACOUSTIC TRAPPING WITH SPECTRAL HOLOGRAMS

A superposition of sound waves at the same frequency can be expressed in the form of Eq. (1), with u(r) and  $\varphi(r)$  representing the amplitude and the phase of the associated interference pattern, respectively. This approach has been used to create holographic acoustic traps [7,15–19], by superposing waves of the same frequency emanating from large arrays of sources. These holographic acoustic trapping patterns can be changed over time by updating the signals emitted by the transducers to produce the desired time-dependent amplitude and phase patterns, u(r, t) and  $\varphi(r, t)$  [19].

Alternatively, time-varying acoustic force landscapes can be created by superposing steady sound waves at different frequencies; the resulting beats manifest as slow time variations of the Gor'kov potential  $U_G(\mathbf{r},t)$  [20]. The spectral content of a polyphonic superposition can supplement the spatiotemporal variations in a standard acoustic hologram to create dynamic acoustic traps using comparatively simple hardware. We refer to this more expansive approach to dynamic wavefront shaping as "spectral holography."

To illustrate the opportunities created by spectral holography, we demonstrate programmable transport along one spatial dimension using force landscapes created with two acoustic pixels. Our experimental system, illustrated in Fig. 1, was introduced by Marzo, Barnes, and Drinkwater [21] and consists of two banks of ultrasonic transducers (Murata MA40S4S, 10 mm in diameter) operating in air at a nominal frequency of 40 kHz. Each bank consists of 36 transducers arranged in concentric hexagonal rings of 6, 12, and 18 transducers that are ganged together to act as a single acoustic pixel. The transducers that make up each acoustic pixel are mounted on a three-dimensional-printed spherical cap and are oriented to launch waves toward the center of the sphere. Each acoustic pixel is driven by a waveform synthesizer (Stanford

Research Systems, DS345) with an amplitude up to  $10~V_{pp}$ . The two synthesizers are synchronized to a common time base to ensure that the two pixels are driven with a stable relative phase.

The two curved transducer banks share a common center, as depicted in Fig. 1(b). The caps therefore define a cylindrical section of a spherical cavity of diameter  $H=10\,\mathrm{cm}$ . The boundaries of this cavity are the top and bottom transducer banks.

Previous studies have described the traveling waves projected by the two acoustic pixels using finite-element modeling [21]. To better illustrate the principles of spectral holography, we instead adopt a simplified analytic model for the pressure waves along the central vertical axis,

$$p_1(z,t) \approx p_0 e^{ik_1 z + i\omega_1 t} \tag{6a}$$

and

$$p_2(z,t) \approx p_0 e^{ik_2 z - i\omega_2 t},\tag{6b}$$

where  $p_0$  is the common pressure amplitude,  $\omega_1$  and  $\omega_2$  are the driving frequencies, and  $k_1$  and  $k_2$  are the corresponding wave numbers. These counterpropagating waves interfere within the cavity to create alternating nodes and antinodes of the pressure field along the central axis.

# A. Diphonic acoustic conveyor

If both sources project waves at the same frequency,  $\omega_1 = \omega_2 = \omega$ , their interference creates a standing wave with axial nodes separated by half a wavelength. Each node acts as a potential energy well for small particles that are denser and less compressible than the medium, such as the airborne expanded polystyrene bead shown in Fig. 1(a). Detuning the two sources by  $\Delta\omega \ll \omega$  so that  $\omega_1 = \omega - \Delta\omega/2$  and  $\omega_2 = \omega + \Delta\omega/2$  creates beats in the axial pressure field,

$$p(z,t) = 2p_0 \cos\left(kz - \frac{\Delta\omega}{2}t\right) \cos\left(\frac{\Delta\omega}{2c_m}z - \omega t\right), \quad (7)$$

that manifest themselves as motion of the time-averaged axial force field,

$$\mathbf{F}_{a}(z,t) = F_{0}(\omega) \sin(2kz - \Delta\omega t)\hat{z}, \tag{8}$$

after substitution into Eq. (4). The prefactor

$$F_0(\omega) = (A - 2B)kp_0^2$$
 (9)

is positive for dense incompressible particles, which therefore tend to be trapped at the nodes of the pressure field. The entire force landscape moves along  $\hat{z}$  at a steady speed,

$$v_c = c_m \frac{\Delta \omega}{2\omega},\tag{10}$$

that is proportional to the detuning  $\Delta\omega$ . Setting aside complications due to inertia and drag [22–25], trapped particles should travel along with the landscape,

$$z_p(t) \approx z_n(t)$$
 (11)

where  $z_n(t) = z_n(0) + v_c t$  is the position of the *n*th pressure node at time *t*. This type of traveling force landscape is known

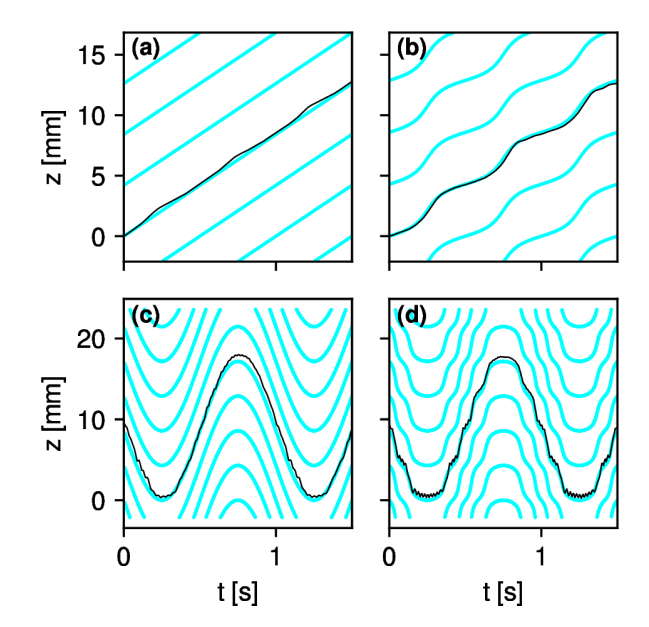


FIG. 2. Measured trajectories (black curves) for a 2 mm in diameter EPS bead being transported through air by the instrument shown in Fig. 1. (a) and (b) Unidirectional transport in a diphonic acoustic conveyor. (c) and (d) Bidirectional transport in a polyphonic acoustic scanner. Measurements are compared with predictions of Eq. (17) for  $\epsilon_0=0.38$  (cyan curves). (b) and (d) Tuning the carrier frequency to a cavity resonance at  $f=\omega/(2\pi)=(40.0\pm0.1)\,\mathrm{kHz}$  creates a standing wave that modulates the trajectory. (a) and (c) Detuning to  $f=40.7\,\mathrm{kHz}$  suppresses the standing wave. Conveyor:  $\Delta f=\Delta\omega/(2\pi)=2\,\mathrm{Hz}$ . Scanner:  $\Delta\phi=720\,\pi$ .

as a "conveyor" [21,26–30] and is the simplest example of a spectral hologram.

This principle previously has been used to transport particles through water in pseudostanding waves created with counterpoised plane-wave sources [30–32] and by sweeping the frequency in a resonant cavity [33]. The same sort of linear transport can be implemented in air using the system depicted in Fig. 1. The system in that case is underdamped, and the resulting motion reveals features of spectral holography that have not previously been described.

The data in Fig. 2(a) demonstrate an acoustic conveyor transporting a millimeter-scale bead through air. The 2-mm-diameter particle is composed of type II expanded polystyrene (EPS) foam with a measured [25] mass density of  $\rho_p = (30.5 \pm 0.2) \,\mathrm{kg} \,\mathrm{m}^{-3}$  and an estimated [34] compressibility of  $\kappa_p = 0.2 \,\mathrm{MPa}^{-1}$ . These values correspond to dimensionless coupling constants near unity:  $f_0 = 0.97$  and  $f_1 = 0.93$ .

The particle's trajectory is recorded at 170 frames/s with a monochrome video camera (FLIR, Blackfly S USB3) whose 5-ms exposure time is fast enough to avoid motion blurring given the system magnification of 61  $\mu$ m/pixel. Each frame in a video sequence is thresholded with Otsu's method, and the particle's position is computed as the center of mass of the resulting simply-connected cluster of foreground pixels. The image of a typical particle yields a 1000-pixel cluster whose axial centroid  $z_p(t)$  can be located with an estimated accuracy [25] of  $\Delta z_p = 0.17$  pixel = 10  $\mu$ m, which suffices for our application.

#### B. Polyphonic acoustic scanner

More sophisticated modes of transport can be achieved with more sophisticated superpositions of tones. Such a generalized conveyor, which we call a "scanner," can be implemented as the superposition of waves from two sources, as depicted in Fig. 1(b), with time-varying relative phase,

$$p_1(t) = p_0 e^{i\omega t} \tag{12a}$$

$$p_2(t) = p_0 e^{i\varphi(t)} e^{-i\omega t}$$
. (12b)

Such a superposition creates a time-averaged force landscape,

$$\mathbf{F}_{a}(z,t) = F_{0}(\omega) \sin[2kz - \varphi(t)] \hat{z}, \tag{13}$$

whose traps travel along  $\hat{z}$  as

$$z_n(t) = z_n(0) - \frac{1}{2k}\varphi(t).$$
 (14)

The resulting motion is slow in the sense that relevant variations in the relative phase satisfy  $|\dot{\varphi}| \ll \omega$ , where the dot refers to a derivative with respect to time. Any faster variations are suppressed in theory by the implicit time average in Eq. (4) and physically by viscous drag and the particle's inertia.

Active control of the relative phase  $\varphi(t)$  has been used in the context of holographic optical trapping to project optical conveyors [26] and optical tractor beams [28], and more recently has been used to demonstrate acoustic conveyors [21]. Rather than actively sweeping the phase, however, we instead can decompose  $\varphi(t)$  into its spectral components and use those to create a scanner that operates in steady state without active intervention. For example, a sinusoidal scanner described by  $\varphi(t) = \Delta \phi \sin(\Omega t)$  can be implemented through the Jacobi-Anger identity

$$p_2(t) = p_0 \sum_{n=-\infty}^{\infty} J_n(\Delta \phi) e^{i(n\Omega - \omega)t}, \qquad (15)$$

which specifies the frequencies needed to implement the scanner and their relative amplitudes. A working example can be projected with just the first few orders,  $n \in [-4, 4]$ . The resulting spectral hologram then transports trapped objects back and forth continuously and smoothly without active intervention. The data in Fig. 2(c) show such a scanner in action.

# C. Spectral superposition of static and dynamic landscapes

Acoustic pixels are actively driven transducers. As a consequence, they not only project sound waves but also act as absorbing boundary conditions for incident waves [35]. This feature has not been emphasized in previous acoustic-trapping studies [21]. Active cancellation of reflections enables the counterpoised acoustic pixels in an instrument such as the example in Fig. 1 to create acoustic traps by straightforward superposition, even when the cavity dimension H is not an integer multiple of the wavelength.

In practice, acoustic pixels reflect a small proportion,  $\epsilon_0$ , of incident sound waves. Reflections contribute to the force landscape by forming standing waves within the cavity whose amplitude can be controlled through the choice of  $\omega$ . The associated force landscape, therefore, has both time-varying and stationary components,

$$\boldsymbol{F}(\boldsymbol{r},t) = \boldsymbol{F}_a(\boldsymbol{r},t) + \boldsymbol{F}_s(\boldsymbol{r}), \tag{16a}$$

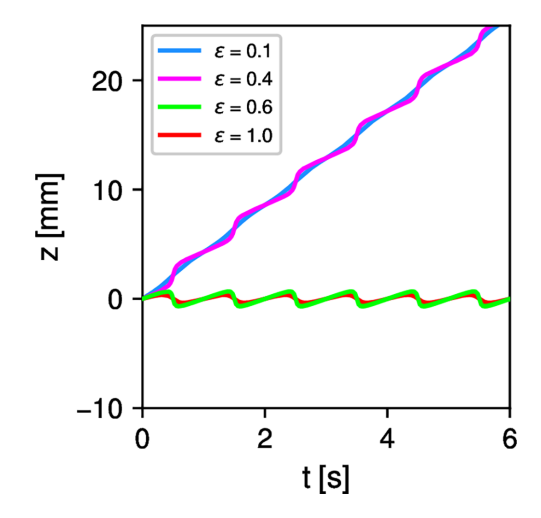


FIG. 3. Simulated trajectories,  $z_p(t)$ , of the particle from Fig. 2 traveling through air in an acoustic conveyor as a function of the acoustic levitator's effective reflection coefficient  $\epsilon(\omega)$ . In all cases, the acoustic conveyor operates at detuning  $\Delta f = \Delta \omega/(2\pi) = 1$  Hz. Tuning the carrier frequency  $\omega$  increases the reflection coefficient from  $\epsilon = 0.1$  to  $\epsilon = 1$ . The particle is trapped in the standing wave when  $\epsilon > 0.5$  and is set into oscillation by the conveyor's periodic forcing. The particle travels with the conveyor for  $\epsilon < 0.5$  although its trajectory is perturbed by the static standing wave.

where the standing-wave contribution is approximately

$$F_s(\mathbf{r}) \approx 2 \epsilon(\omega) F_0(\omega) \sin(2kz) \hat{z}.$$
 (16b)

The factor of 2 in Eq. (16b) accounts for the independent contributions from each of the pixels. The depth of the stationary landscape's modulation,

$$\epsilon(\omega) = \epsilon_0 \cos\left(\frac{2H}{c_m}\omega\right),$$
 (16c)

is proportional to the acoustic pixels' reflection coefficient  $\epsilon_0$  and can be tuned by adjusting the carrier frequency. For the cavity depicted in Fig. 1, we find that particle trajectories are consistent with  $\epsilon_0 = 0.38(2)$ . The overall scale of the stationary force landscape is set by  $F_0(\omega)$ , which is given by Eq. (9).

If the reflection coefficient is large enough,  $\epsilon_0 > 0.5$ , the central frequency can be tuned so that  $2\epsilon(\omega) > 1$ . In that case, the standing wave exerts enough force to trap the particle, and the dynamic landscape acts as a time-dependent perturbation. Representative trajectories for this mode of motion are plotted in Fig. 3 as a function of  $\epsilon(\omega)$ .

In the opposite limit of weak reflections,  $\epsilon(\omega)$  < 0.5, the particle is transported by the moving conveyor across the stationary landscape. The nodes then trace out trajectories,

$$z_n[t|\epsilon(\omega)] = z_n(0) - \frac{1}{k} \arctan\left[\frac{\epsilon(\omega) - 1}{\epsilon(\omega) + 1} \tan\left(\frac{\varphi(t)}{2}\right)\right],$$
(17)

that reduce to Eq. (14) when  $\epsilon(\omega) = 0$ . This mode of motion also is plotted in Fig. 3 and is consistent with the perturbed trajectories observed experimentally in Figs. 2(b) and 2(d).

The particles' trajectories increasingly deviate from the traps' trajectories as  $\epsilon(\omega)$  approaches 1/2 and the trajectories

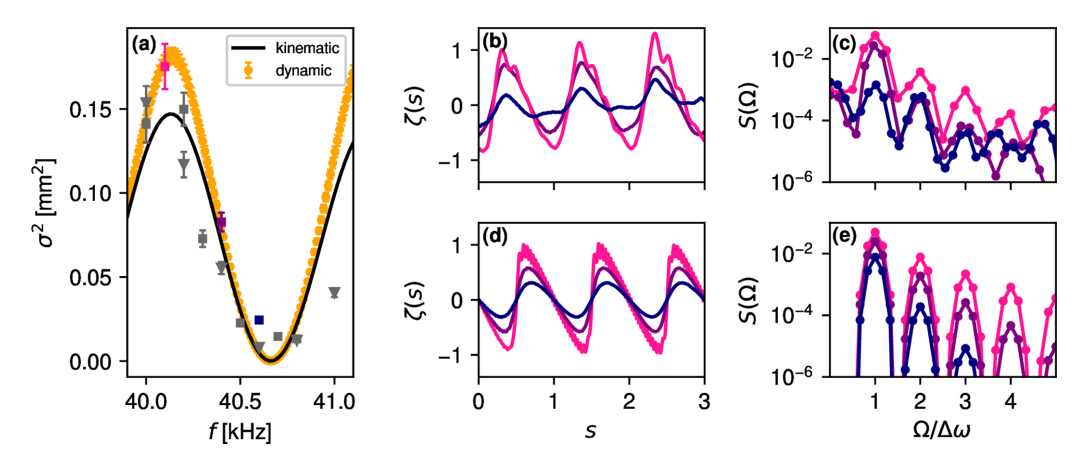


FIG. 4. Transport properties of a 2 mm in diameter EPS sphere moving through air in a diphonic acoustic conveyor. (a) Variance of the particle's departures from the conveyor's planned trajectory as a function of the acoustic trap's carrier frequency,  $f = \omega/(2\pi)$ . Measured values are computed with Eq. (18) and are plotted as discrete points. Solid curves denote analytic predictions of Eq. (17) (black curve) and numerical solutions to Eq. (22) (orange curve). (b) Typical measured trajectories scaled according to Eq. (21) and colored to match corresponding points in panel (a). (c) Power spectra of the trajectories in panel (b) showing the growth of harmonics in the particle's trajectory as the depth of modulation increases. (d) and (e) Numerical solutions of Eq. (22) for the same set of conditions. Conveyor detuning frequency:  $\Delta f = \Delta \omega/2\pi = 2 \, \text{Hz}$ .

become increasingly sinuous. We quantify these deviations with the kinematic variance

$$\sigma^{2}(\omega) = \frac{1}{T} \int_{0}^{T} [z_{p}(t) - z_{n}(t)]^{2} dt,$$
 (18)

which is plotted as a function of the carrier frequency  $\omega$  in Fig. 4(a). Measurements are compared with the prediction obtained by setting  $z_p(t) = z_n(t|\epsilon(\omega))$ , which is plotted as a solid curve. The kinematic model is consistent with the measurement when the carrier frequency is tuned away from the cavity resonance so that the particle travels smoothly at constant speed. Tuning to the cavity resonance at  $f = 40.2 \, \text{kHz}$  maximizes the particle's acceleration and increases deviations between the trajectories of the particle and the trap. These discrepancies can be resolved by accounting for inertial corrections to the viscous drag acting on the particle.

# IV. ACCOUNTING FOR INERTIA AND DRAG

A trapped particle hews to the trajectory of its acoustic trap if the motion is slow enough to neglect the inertia of the fluid medium [25]. More generally, the equation of motion for a particle of mass  $m_p$ ,

$$m_p \ddot{z}_p = F_a(z_p, t) + F_s(z_p) + F_d(\dot{z}_p, \ddot{z}_p),$$
 (19)

reflects contributions from the active force landscape, the stationary force landscape, and viscous drag, respectively. Equation (19) omits the influence of gravity, whose principal role is to offset the particle's equilibrium position. For the experiments described in Fig. 2, this offset is estimated to be  $\Delta z_p = (80 \pm 1) \, \mu \text{m}$  [25].

The accelerating sphere experiences a drag force that is described by the Basset-Boussinesq-Oseen equation [22,24,36,37],

$$F_{d}(\dot{z}_{p}, \ddot{z}_{p}) = 6\pi \eta_{m} a_{p} \left[ \dot{z}_{p} + \tau \ddot{z}_{p} + \sqrt{\frac{9\tau}{\pi}} \int_{-\infty}^{t} \frac{\ddot{z}_{p}(t')}{\sqrt{t - t'}} dt' \right],$$
(20a)

which accounts for the inertia of the displaced fluid on timescales set by the viscous relaxation time,

$$\tau = \frac{\rho_m}{9\eta_m} a_p^2. \tag{20b}$$

Equation (20) is strictly valid for Reynolds numbers less than unity and yields useful results for Reynolds numbers less than 100 [36,37].

The history dependence of the drag complicates an analytic formulation of the transport properties for a general spectral hologram. To illustrate the challenge, we consider the comparatively simple case of a particle moving under the influence of an acoustic conveyor. Competition between the active and stationary force landscapes causes the particle to oscillate at the beat frequency  $\Delta\omega$  about the moving trap's position. We therefore define the dimensionless displacement in the comoving frame,

$$\zeta(t) = 2kz_p(t) - \begin{cases} \Delta\omega t, & \epsilon(\omega) < 0.5, \\ 0, & \epsilon(\omega) > 0.5. \end{cases}$$
 (21)

Applying Eqs. (19) and (20) then yields the following deceptively simple dimensionless equation of motion,

$$\zeta'' + b\zeta' + \zeta = \tilde{\epsilon} \sin\left(\zeta - \frac{\Delta\omega}{\omega_0}s\right),$$
 (22)

where primes denote derivatives with respect to the dimensionless time  $s = \omega_0 t$ . Equation (22) describes a wave-driven oscillator [10] whose exceptionally rich phenomenology only recently has been brought to light. Wave-driven oscillators differ from more familiar nonlinear dynamical systems, such as the Duffing oscillator [38,39], because their spatial nonlinearity is irreducibly coupled to the time dependence of the driving.

The effective driving strength in Eq. (22),

$$\tilde{\epsilon}(\omega) = \begin{cases} 2\epsilon(\omega), & \epsilon(\omega) < 0.5, \\ \frac{1}{2\epsilon(\omega)}, & \epsilon(\omega) > 0.5, \end{cases}$$
 (23)

can be varied over the range  $\tilde{\epsilon}(\omega) \in [0, 1]$  by adjusting the carrier frequency relative to the cavity resonance. Similarly, the natural frequency,

$$\omega_0(\omega) = \sqrt{\frac{2kF_0}{m}} \begin{cases} 1, & \epsilon(\omega) < 0.5, \\ \sqrt{2\epsilon(\omega)}, & \epsilon(\omega) > 0.5, \end{cases}$$
(24)

and the drag coefficient,

$$b(\omega) = \frac{6\pi \eta_m a_p}{m \omega_0} \begin{cases} 1, & \epsilon(\omega) < 0.5, \\ [2\epsilon(\omega)]^{-1}, & \epsilon(\omega) > 0.5, \end{cases}$$
(25)

both depend on cavity tuning when  $\epsilon(\omega) > 0.5$ .

Equations (24) and (25) incorporate the inertial corrections from Eq. (20) by introducing the dynamical mass [22,23,25],

$$m(\Delta\omega) = m_p \left\{ 1 + \frac{1}{2} \frac{\rho_m}{\rho_p} \left[ 1 + \frac{9}{2} \frac{\delta(\Delta\omega)}{a_p} \right] \right\}, \tag{26a}$$

under the simplifying assumption the particle oscillates harmonically at the driving frequency  $\Delta\omega$ . The sphere's effective mass is increased in this approximation by the mass of the fluid in a Prandtl-Schlichting boundary layer of thickness [22]

$$\delta(\Delta\omega) = \sqrt{\frac{2\eta_m}{\rho_m} \frac{1}{\Delta\omega}}.$$
 (26b)

This correction has been demonstrated to quantitatively model the damped oscillations of a particle levitated in a static acoustic trap [25]. For particles moving in an acoustic conveyor, the dynamic model more accurately accounts for the magnitude of measured fluctuations, as can be seen in Fig. 4(a).

Measured acoustic-conveyor trajectories in Fig. 4(b) and their power spectra in Fig. 4(c) are reproduced reasonably well by the numerical solutions of Eq. (22) that are plotted in Figs. 4(d) and 4(e). These examples illustrate the effect of tuning the carrier frequency on the amplitude and harmonic content of the particle's dynamic response. Values of  $F_0$  and  $m_0$  used for the numerical solutions are obtained from measured trajectories using the analytical approach described in Ref. [25]. The power spectra are computed as

$$S(\Omega) = \left| \int_0^1 \zeta(s) W(s) e^{-i\Omega s} ds \right|^2, \tag{27}$$

using the Blackman-Harris window function W(s). The wave-driven oscillator responds most strongly at the driving frequency  $\Omega = \Delta \omega$ . Increasingly much power is directed into harmonics of that driving frequency as the depth of modulation increases. Agreement between the measured and computed power spectra illustrates the utility of the Basset-Boussinesq-Oseen (BBO) equation for interpreting the behavior of wave-driven oscillators created with sound. At the same time, the presence of strong harmonics suggests even better agreement could be attained by seeking self-consistent solutions to the equation of motion, including the BBO correction described in Eq. (20).

More generally, the wave-driven oscillator has been shown [10] to respond at both harmonics and subharmonics of the driving frequency and to undergo transitions between subharmonic states depending on the strength of the driving  $\tilde{\epsilon}(\omega)$ , the strength of the damping  $b(\omega)$ , and the relationship between the driving frequency  $\Delta \omega$  and the oscillator's natural frequency  $\omega_0$ . Transitions between subharmonic states feature both period-doubling routes to chaos and Fibonacci cascades [10]. No complete description of the wave-driven oscillator is yet available, even in the weak-driving regime,  $\tilde{\epsilon} < 1$ . Previous experimental and numerical studies [10], furthermore, have neglected the inertial corrections described by Eq. (20) that are likely to have influenced their results. Future studies of the wave-driven oscillator and related dynamical systems would benefit both from the streamlined experimental implementation afforded by spectral holography and from the analytical approach discussed here.

#### V. DISCUSSION

Spectral holographic trapping uses interference among waves at multiple frequencies to create time-averaged force landscapes that evolve dynamically on the inertial timescales of trapped objects. Spatiotemporal control afforded by the frequency content of the projected waves reduces the complexity of acoustic manipulation systems by replacing the many spatial degrees of freedom required for conventional monotonic holographic projection. Spectral holography therefore allows complex force landscapes to be generated with small numbers of acoustic pixels. We have demonstrated two archetypal examples, a unidirectional conveyor created with two frequencies and a bidirectional scanner created with nine. We also have shown that tuning the carrier frequency to cavity resonances can usefully implement a superposition of dynamic and static force fields with no additional complexity. In the case of an acoustic conveyor, this superposition implements a wave-driven oscillator whose exceedingly rich dynamical properties emerge from an interplay among the acoustic force field, the particle's inertia, and viscous drag in the supporting medium. This study also highlights the importance of accounting for the fluid's inertia when planning and interpreting the motions of particles in acoustic force landscapes.

The combination of rich spectral control and analytic dynamical modeling expands the prospects for dexterous acoustic manipulation of macroscopic materials. The present study has focused on the dynamics of individual particles in spectral holograms created within cavities. Additional opportunities can be imagined for free-space manipulation with traveling waves and for self-organization guided by wave-mediated interactions in many-body systems immersed in spectral holograms.

# ACKNOWLEDGMENT

This work was supported by the National Science Foundation under Award No. DMR-2104837.

of cells and particles, Chem. Soc. Rev. **36**, 492 (2007).

<sup>[1]</sup> T. Laurell, F. Petersson, and A. Nilsson, Chip integrated strategies for acoustic separation and manipulation

- [2] D. Foresti, M. Nabavi, M. Klingauf, A. Ferrari, and D. Poulikakos, Acoustophoretic contactless transport and handling of matter in air, Proc. Natl. Acad. Sci. USA 110, 12549 (2013).
- [3] M. M. Burns, J.-M. Fournier, and J. A. Golovchenko, Optical binding, Phys. Rev. Lett. 63, 1233 (1989).
- [4] K. Dholakia and P. Zemánek, *Colloquium:* Gripped by light: Optical binding, Rev. Mod. Phys. **82**, 1767 (2010).
- [5] M. X. Lim, B. VanSaders, A. Souslov, and H. M. Jaeger, Mechanical properties of acoustically levitated granular rafts, Phys. Rev. X 12, 021017 (2022).
- [6] M. A. Abdelaziz, J. A. Díaz A., J.-L. Aider, D. J. Pine, D. G. Grier, and M. Hoyos, Ultrasonic chaining of emulsion droplets, Phys. Rev. Res. 3, 043157 (2021).
- [7] A. Marzo and B. W. Drinkwater, Holographic acoustic tweezers, Proc. Natl. Acad. Sci. USA 116, 84 (2019).
- [8] Y. Ochiai, T. Hoshi, and J. Rekimoto, Three-dimensional midair acoustic manipulation by ultrasonic phased arrays, PLoS One 9, e97590 (2014).
- [9] D. G. Grier, A revolution in optical manipulation, Nature (London) 424, 810 (2003).
- [10] M. A. Abdelaziz and D. G. Grier, Dynamics of an acoustically trapped sphere in beating sound waves, Phys. Rev. Res. 3, 013079 (2021).
- [11] H. Bruus, Acoustofluidics 2: Perturbation theory and ultrasound resonance modes, Lab Chip 12, 20 (2012).
- [12] M. A. Abdelaziz and D. G. Grier, Acoustokinetics: Crafting force landscapes from sound waves, Phys. Rev. Res. 2, 013172 (2020).
- [13] H. Bruus, Acoustofluidics 7: The acoustic radiation force on small particles, Lab Chip 12, 1014 (2012).
- [14] P. C. Chaumet and M. Nieto-Vesperinas, Time-averaged total force on a dipolar sphere in an electromagnetic field, Opt. Lett. 25, 1065 (2000).
- [15] K. Melde, H. Kremer, M. Shi, S. Seneca, C. Frey, I. Platzman, C. Degel, D. Schmitt, B. Schölkopf, and P. Fischer, Compact holographic sound fields enable rapid one-step assembly of matter in 3D, Sci. Adv. 9, eadf6182 (2023).
- [16] K. Melde, A. Mark, T. Qiu, and P. Fischer, Holograms for acoustics, Nature (London) 537, 518 (2016).
- [17] M. D. Brown, Phase and amplitude modulation with acoustic holograms, Appl. Phys. Lett. 115, 053701 (2019).
- [18] T. Fushimi, K. Yamamoto, and Y. Ochiai, Acoustic hologram optimisation using automatic differentiation, Sci. Rep. 11, 12678 (2021).
- [19] A. Marzo, S. Seah, B. Drinkwater, D. Sahoo, B. Long, and S. Subramanian, Holographic acoustic elements for manipulation of levitated objects, Nat. Commun. 6, 8661 (2015).
- [20] Q. Wang, A. Riaud, J. Zhou, Z. Gong, and M. Baudoin, Acoustic radiation force on small spheres due to transient acoustic fields, Phys. Rev. Appl. 15, 044034 (2021).
- [21] A. Marzo, A. Barnes, and B. W. Drinkwater, TinyLev: A multiemitter single-axis acoustic levitator, Rev. Sci. Instrum. 88, 085105 (2017).
- [22] L. D. Landau and E. M. Lifshitz, *Fluid Mechanics* (Elsevier, Amsterdam, 1987).

- [23] M. Settnes and H. Bruus, Forces acting on a small particle in an acoustical field in a viscous fluid, Phys. Rev. E 85, 016327 (2012).
- [24] D. Baresch, J.-L. Thomas, and R. Marchiano, Observation of a single-beam gradient force acoustical trap for elastic particles: Acoustical tweezers, Phys. Rev. Lett. 116, 024301 (2016).
- [25] M. Morrell and D. G. Grier, Acoustodynamic mass determination: Accounting for inertial effects in acoustic levitation of granular materials, Phys. Rev. E 108, 064903 (2023).
- [26] T. Čižmár, V. Garcés-Chávez, K. Dholakia, and P. Zemánek, Optical conveyor belt for delivery of submicron objects, Appl. Phys. Lett. 86, 174101 (2005).
- [27] T. Čižmár and K. Dholakia, Tunable Bessel light modes: engineering the axial propagation, Opt. Express 17, 15558 (2009)
- [28] D. B. Ruffner and D. G. Grier, Optical conveyors: A class of active tractor beams, Phys. Rev. Lett. 109, 163903 (2012).
- [29] J. Li, C. Shen, T. J. Huang, and S. A. Cummer, Acoustic tweezer with complex boundary-free trapping and transport channel controlled by shadow waveguides, Sci. Adv. 7, eabi5502 (2021).
- [30] M. Kandemir, M. Beelen, R. Wagterveld, D. Yntema, and K. Keesman, Dynamic acoustic fields for size selective particle separation on centimeter scale, J. Sound Vib. 490, 115723 (2021).
- [31] G. Whitworth, M. Grundy, and W. Coakley, Transport and harvesting of suspended particles using modulated ultrasound, Ultrasonics **29**, 439 (1991).
- [32] G. Simon, Y. Pailhas, M. A. B. Andrade, J. Reboud, J. Marques-Hueso, M. P. Y. Desmulliez, J. M. Cooper, M. O. Riehle, and A. L. Bernassau, Particle separation in surface acoustic wave microfluidic devices using reprogrammable, pseudo-standing waves, Appl. Phys. Lett. 113, 044101 (2018).
- [33] N. Jeger-Madiot, X. Mousset, C. Dupuis, L. Rabiet, M. Hoyos, J.-M. Peyrin, and J.-L. Aider, Controlling the force and the position of acoustic traps with a tunable acoustofluidic chip: Application to spheroid manipulations, J. Acoust. Soc. Am. 151, 4165 (2022).
- [34] W. Chen, H. Hao, D. Hughes, Y. Shi, J. Cui, and Z.-X. Li, Static and dynamic mechanical properties of expanded polystyrene, Mater. Des. 69, 170 (2015).
- [35] P. Mokrý, E. Fukada, and K. Yamamoto, Sound absorbing system as an application of the active elasticity control technique, J. Appl. Phys. **94**, 7356 (2003).
- [36] M. R. Maxey and J. J. Riley, Equation of motion for a small rigid sphere in a nonuniform flow, Phys. Fluids 26, 883 (1983).
- [37] P. M. Lovalenti and J. F. Brady, The hydrodynamic force on a rigid particle undergoing arbitrary time-dependent motion at small Reynolds number, J. Fluid Mech. **256**, 561 (1993).
- [38] M. A. Andrade, T. S. Ramos, F. T. Okina, and J. C. Adamowski, Nonlinear characterization of a single-axis acoustic levitator, Rev. Sci. Instrum. 85, 045125 (2014).
- [39] T. Fushimi, T. L. Hill, A. Marzo, and B. W. Drinkwater, Nonlinear trapping stiffness of mid-air single-axis acoustic levitators, Appl. Phys. Lett. 113, 034102 (2018).